water

MDPI

Article

Strontium Removal in Seawater by Means of Composite Magnetic Nanoparticles Derived from Industrial Sludge

Yao-Jen Tu [1], Chen-Feng You [2,3], Zhonghao Zhang [1,*], Yanping Duan [1], Jing Fu [1] and Di Xu [1]

[1] Institute of Urban Study, Shanghai Normal University, No. 100 Guilin Rd., Shanghai 200234, China; yjtu@shnu.edu.cn (Y.-J.T.); duanyanping@shnu.edu.cn (Y.D.); tristar@shnu.edu.cn (J.F.); xudishnu@shnu.edu.cn (D.X.)

[2] Earth Dynamic System Research Center, National Cheng-Kung University, No 1, University Road, Tainan City 701, Taiwan; cfy20@mail.ncku.edu.tw

[3] Department of Earth Sciences, National Cheng-Kung University, No 1, University Road, Tainan City 701, Taiwan

* Correspondence: zzh87@shnu.edu.cn; Tel.: +86-21-6432-2571

Academic Editor: Maria Filomena Camões

Received: 13 June 2016; Accepted: 3 August 2016; Published: 19 August 2016

Abstract: Novel composite magnetic nanoparticles ($CuFe_2O_4$) were synthesized from industrial sludge by acid leaching, chemical exchange, and ferrite processes in the laboratory. For the first time, these products were applied to investigate the Sr adsorption kinetics and the related thermodynamics in seawater. Rapidly enhanced Sr adsorption was observed when the solution pH changed from 2.61 to 10.25. The maximum adsorption capacity was 23.04 $mg \cdot g^{-1}$ at 318 K (pH 10.25). Sr adsorption decreased with the increase of the ionic strength from 0.01 to 0.5 $mol \cdot L^{-1}$ at pH 2.61–pH 10.25, indicating that the outer-sphere mechanism was involved in the Sr adsorption at the pH interval. This reaction is spontaneous and endothermic, as indicated by the negative change in the standard free energy (ΔG° = −5.68, −6.45, and −7.23 $kJ \cdot mol^{-1}$ at 298, 308, and 318 K, respectively) and positive ΔH° value (2.11 $kJ \cdot mol^{-1}$). The positive ΔS° (9.38 $mol^{-1} \cdot K^{-1}$) further confirms that the randomness increased at the solid-solution interface during adsorption. These new results indicate that the composite magnetic nanoparticles can be used for the removal of radiogenic ^{90}Sr nuclide in seawater that was released after the 3/11 earthquake offshore of Japan.

Keywords: composite magnetic particles; industrial sludge; seawater; Sr adsorption; kinetics and thermodynamics

1. Introduction

Strontium (Sr), the fifteenth most abundant element on Earth, is one of the major fission products present in the wastewater from nuclear power plants and spent nuclear fuel reprocessing [1,2]. In addition to 31 unstable isotopes, Sr has four major naturally occurring stable isotopes: ^{84}Sr, ^{86}Sr, ^{87}Sr, and ^{88}Sr. The longest-lived unstable isotope is ^{90}Sr, with a half-life of 28.9 years [3]. Sr has a variety of medical, commercial, and industrial applications [4]. For instance, Sr has been used in optical materials and as an oxygen eliminator in electron tubes. Nevertheless, a high Sr concentration can be detected in seawater, industrial wastewater, and even in surface water because of improper Sr-bearing waste treatment.

Moreover, owing to its chemical similarity to calcium (Ca), Sr follows the path of Ca in the food chain, enters the human body, and is incorporated into bones [5]. If radioisotope ^{90}Sr enters bone, it irradiates localized tissues, leading to leukemia, bone sarcoma, and other chronic problems [6,7]. Therefore, Sr is considered one of the most dangerous radionuclides to human health due to its

high solubility, transferability, and easy assimilation [8,9]. The removal of Sr from water is therefore a critical issue.

The average concentration of Sr in surface water, groundwater, and seawater is 1.1, 0.8, and 8.0 $mg \cdot L^{-1}$, respectively [10]. However, much higher Sr (tens of $mg \cdot L^{-1}$) can be found in aquatic systems because of anthropogenic influences, such as the wastewater generated from nuclear power plants. Hence, a rapid, effective and economical method to concentrate and separate the Sr ions from aqueous solutions is an important topic for both aquatic ecosystems and human health.

Some traditional technologies, including ion exchange, adsorption, chemical precipitation, and membrane filtration, have been proposed to remove Sr from aqueous solutions [11–16]. However, these technologies are impractical owing to the defects of low efficiency, high cost, and secondary contamination. For example, membrane technology has high treatment cost because of the frequent change of membranes. Chemical precipitation generates a large amount of fluffy sludge that consequently causes an increase of treatment cost.

"Adsorption" is regarded as a fast and effective approach to remove metal ions from aqueous solutions [17–20]. Several adsorbents have been investigated to remove Sr from water, such as ammonium molybdophosphate polyacrylonitrile [13], hydrous ferric oxide [21], and dolomite [22]. However, the low recovery of the adsorbents is a problem in the regeneration systems.

Composite magnetic particles ($CuFe_2O_4$) with the spinel structure have a cubic, close-packed arrangement of oxygen ions with Cu^{2+} and Fe^{3+} ions at two different crystallographic sites [23]. Owing to their high saturation magnetism and specific surface area, these composite magnetic particles are widely applied in contaminant removal [18,24,25]. Nevertheless, there is lack of information about Sr removal from aqueous solution by low-cost, composite magnetic particles ($CuFe_2O_4$). This process is easily controlled, and the particles can be quickly separated from the water after adsorption.

This study investigates Sr removal using composite magnetic particles manufactured from sludge from the printed circuit board (PCB) industry. The previous study noted that Cu powder could be recycled from PCB sludge through a combination of acid leaching and chemical exchange [26]. Then, a ferrite process ensures that not only the supernatant but also the sludge can meet the environmental law requirements. The sludge manufactured from the ferrite process is considered as general industrial waste because of its high stability in natural environments.

This study aims to investigate the influence of the adsorption parameters, such as competitive ions, pH, ionic strength, and temperature, on composite magnetic particles. The values from thermodynamic and kinetic studies of Sr were also investigated and discussed. The information obtained indicates great potential for developing a cost-effective adsorbent to immobilize Sr using composite magnetic particles.

2. Materials and Methods

2.1. Chemicals

All chemicals were of analytical grade and were used as received without further purification. The Sr^{2+} stock solutions were prepared using strontium chloride ($SrCl_2 \cdot 6H_2O$), which was purchased from J.T. Baker (Phillipsburg, NJ, USA). Nitric acid (97%) and sodium hydroxide, used to adjust the pH, were obtained from Sigma-Aldrich (Darmstadt, Germany). All solution samples used in the adsorption experiments were prepared from Milli-Q water (Darmstadt, Germany).

2.2. Manufacturing of Composite Magnetic Nanoparticles

The composite magnetic nanoparticles were manufactured from PCB sludge by a combination of acid leaching, chemical exchange, and ferrite process. Our previous work provides the detailed procedure for the preparation of $CuFe_2O_4$ [26]. Acid leaching was performed using 500 g industrial sludge, and 10 L diluted sulfuric acid was added to extract Cu from the solids. Fe^0 was used as the sacrificed metal to substitute Cu^{2+} in the liquid during chemical exchange. To ensure the supernatant qualities reached the effluent standards, the ferrite process was conducted after chemical exchange.

The low-cost, composite magnetic nanoparticles of $CuFe_2O_4$ were manufactured after the ferrite process. The reactions of acid leaching, chemical exchange, and the ferrite process can be expressed as Equations (1)–(3), respectively:

$$Cu - \text{sludge} + H_2SO_4 \rightarrow Cu^{2+} + \text{sludge} \quad (1)$$

$$Fe^0 + Cu^{2+} \rightarrow Fe^{2+} + Cu^0 \quad (2)$$

$$Cu^{2+} + 2Fe^{2+} + 6OH^- + 1/2O_2 \rightarrow CuFe_2O_4 + 3H_2O \quad (3)$$

The adsorbent was collected using a magnetic separation method. The $CuFe_2O_4$ was then washed with Milli-Q water several times until the solution pH was close to 7 (pH 6.80–7.20). The solids were dried at 323 K for 24 h in an oven and were stored for further tests.

2.3. Characterization of the Composite Magnetic Nanoparticles

The characteristics of the composite magnetic nanoparticles used in this study were elucidated using various technologies. The crystal phases were determined by XRD (D8 Advance, Bruker, Karlsruhe, Germany) using graphite monochromatic copper radiation over the 2θ range of 10°–80°. The particle size and the point of zero charge (PZC) of the adsorbent were obtained using a zeta meter (Zetasizer Nano ZS 90, Southborough, MA, USA). The saturation magnetization of the synthesized adsorbent was measured using a Superconducting Quantum Interference Device (SQUID, MPMS-XL7, Quantum Design, San Diego, CA, USA) at 27 °C. The Brunauer–Emmett–Teller (BET) surface areas and the porosity of the adsorbents were obtained from nitrogen adsorption isotherms at 77 K using an ASAP 2010 analyzer (Micromeritics, ASAP 2010, Norcross, GA, USA). The morphology was examined by scanning electron microscopy (SEM, JSM-6330, Tokyo, Japan).

2.4. Batch Adsorption Experiments

Batch experiments were conducted to evaluate the adsorption processes and the equilibrium states of Sr mobilization. The Sr stock solution was prepared by dissolving strontium chloride ($SrCl_2 \cdot 6H_2O$) in Milli-Q water. Working solutions for the experiments were freshly prepared from the stock solution. All batch adsorption experiments were performed according to the following procedures: 10 mL Sr solution and a fixed amount of composite magnetic nanoparticles were poured into a 15 mL centrifuge tube. The centrifuge tubes were placed on a shaft of a rotary shaker after the caps were tightened.

To evaluate the influence of the solution pH and the competitive influence of positive ions on the Sr adsorption, various experiments were performed by adding 0.05 g of the adsorbent into a 15 mL centrifuge tube containing 10 mL of a 10 $mg \cdot L^{-1}$ Sr solution at 298 ± 1 K. The pH of the solutions was adjusted to the designated values (2.61 ± 0.05, 4.29 ± 0.05, 6.98 ± 0.05, 8.79 ± 0.05, 10.25 ± 0.05, and 11.36 ± 0.05) using 0.1 N HNO_3 or NaOH solution. The competitive cations (Mg^{2+}, Ca^{2+}, Ba^{2+}) of the solutions were set to ratios of M/Sr = 0, 5, 10, and 100 (where M represents Mg, Ca, or Ba) at an NaCl ionic strength of 0.5 $mol \cdot L^{-1}$. The ionic strength experiments were conducted under atmospheric conditions. NaCl was used to adjust different ionic strengths (0.01 to 0.5 $mol \cdot L^{-1}$). All equilibrium adsorption experiments were individually conducted by shaking 0.05 g of the composite magnetic nanoparticles with 10 $mg \cdot L^{-1}$ Sr solution using a thermostated shaker at a speed of 30 rpm for 2 h.

The adsorption kinetics for Sr were measured by mixing 10 $mg \cdot L^{-1}$ Sr solution with 0.05 g of the adsorbent and shaking the mixture at pH 10.25 and 298 ± 1 K. The Sr uptake rate of q_t ($mg \cdot g^{-1}$) was determined by Equation (4):

$$q_t = \frac{(C_o - C_t) \times V}{m} \quad (4)$$

where C_0 and C_t are the metal concentrations in liquid phase initially and at time t ($mg \cdot L^{-1}$), respectively; m is the adsorbent amount (g); and V is the volume used in the adsorption process (L).

The Sr concentrations in the filtrate were determined by inductively coupled plasma optical emission spectroscopy (ICP-OES, iCAP 6300, Dreieich, Germany). The amount of Sr adsorbed on the composite magnetic nanoparticles was determined using the differences between the initial and the equilibrium concentrations in the solutions. All experiments provided in this study were performed in triplicate. The relative standard deviation (RSD) of three replicate analyses was lower than 3%. Prior to analysis, the supernatant was acidified with concentrated HNO_3 and stored in acid-washed bottles.

3. Results and Discussion

3.1. Basic Properties of the Adsorbent

The physical/chemical properties of the synthesized adsorbent are presented in Figure 1. Briefly, the XRD pattern (Figure 1a) shows that the crystalline phase of this material matched very well with the $CuFe_2O_4$ standard (Joint Committee on Powder Diffraction Standards (JCPDS) file number 00-025-0283). The SEM image (Figure 1b) shows that the primary size of the particles ranged from 20 to 120 nm. The BET surface area, pore volume, and average pore diameter of the adsorbent were 48.3 $m^2 \cdot g^{-1}$, 0.08 $cm^3 \cdot g^{-1}$, and 13.57 Å, respectively. The point of zero charge (PZC) and the saturation magnetization of the adsorbent were approximately 7.3 (at 0.1 $mol \cdot L^{-1}$ ionic strength) and 62.5 $emu \cdot g^{-1}$, respectively. It should be noted that the surface charge of the adsorbent depends on the activities of ions and electrolyte concentrations (ionic strength). No remnant was detected in the sample, confirming that the synthesized nanoparticles were superparamagnetic. In the experiments, these magnetic nano-particles could be collected within 20 s using a magnet. For more detailed information, please refer to the authors' previous investigation [27].

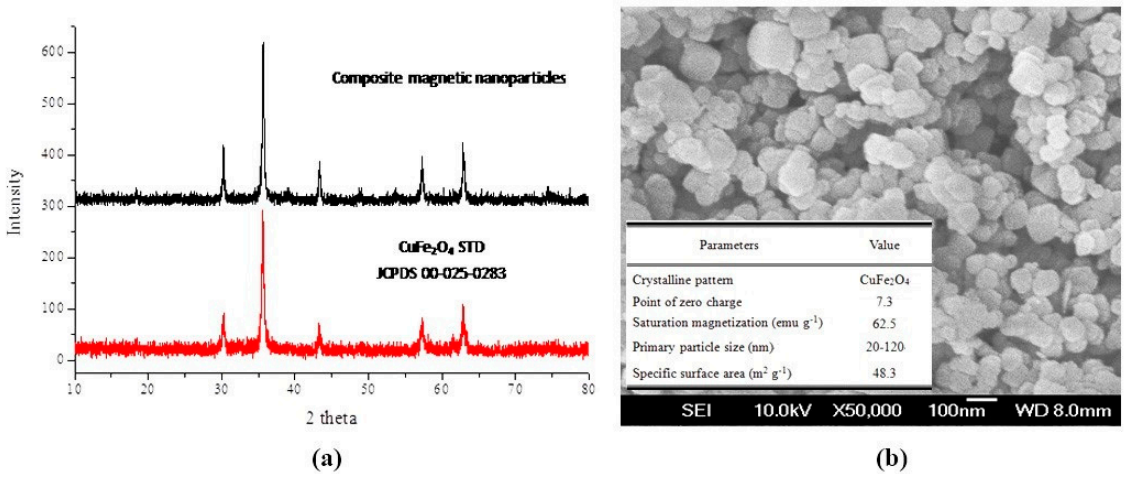

Figure 1. (**a**) XRD spectra; and (**b**) SEM image of the composite magnetic nanoparticles.

3.2. Effect of pH and Competitive Ions

3.2.1. pH Effect

The pH is a critical factor during the adsorption process [28]. The amount of Sr adsorbed onto the composite magnetic nanoparticles at various pHs and ionic strengths is illustrated in Figure 2. The results showed that the sorption curve of Sr in 0.01 $mol \cdot L^{-1}$ NaCl solution at pH < 10 is the highest and that of Sr in 0.5 $mol \cdot L^{-1}$ NaCl solution is the lowest, and no sharp difference was found at pH > 10. This phenomenon indicates that Sr sorption on the composite magnetic nanoparticles is mainly dominated by ion exchange or outer-sphere surface complexation at pH < 10. The ionic strength-independent sorption at pH > 10 suggests that inner-sphere surface complexation or surface precipitation is the main sorption mechanism for Sr uptake on the composite magnetic nanoparticles at high pH values.

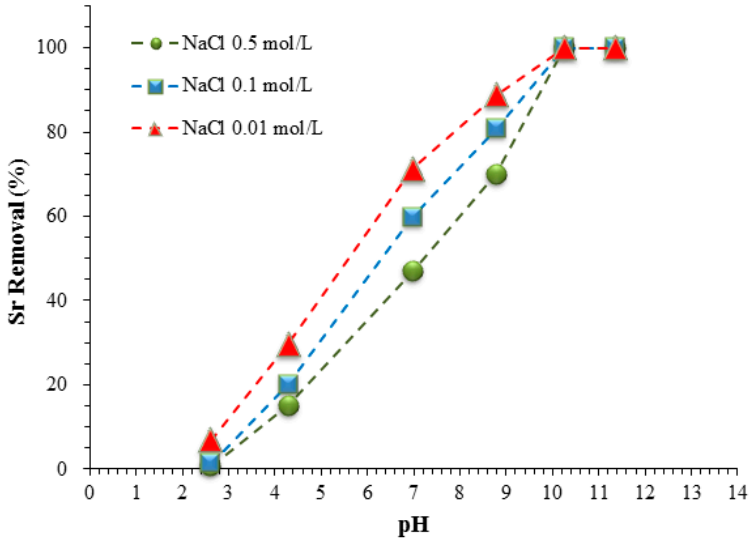

Figure 2. The Strontium (Sr) adsorption by the composite magnetic nanoparticles at various pH values. Conditions: Adsorbent dose 5 g·L^{-1}, *T* 298 K, contact time 120 min, initial Sr concentration 10 mg·L^{-1}.

In addition, rapidly increased Sr removal was observed when the solution pH increased from 2.61 to 10.25 at 298 K. This phenomenon is similar to the results using waste iron oxide BT_1 [29] and BT_9 [30]. Sr^{2+} was the dominant species in solution at pH less than 11; at pH values greater than 11, $Sr(OH)^+$ was dominant [13]. On the other hand, the speciation in solution and the surface charge of the composite magnetic nanoparticles play important roles in Sr adsorption. At higher pH values (in the pH range of 8.79–10.25), there is intrinsic attraction between hydroxyl ions (OH^-) and Sr^{2+}; strong hydroxyl ions may enhance the approach of Sr cations as a consequence of attractive forces.

Additionally, the surface of the adsorbent may be subject to protonation/deprotonation, which relies heavily on the solution pH. As indicated by the PZC of the synthesized composite magnetic nanoparticles (i.e., 7.30), the net surface charge is negative at pH > 7.30, which is beneficial for adsorbing the positive ions. This charge explains the observations of high Sr uptake in more alkaline conditions. An increase of solution pH resulted in a buildup of more negative charges on the adsorbent, leading to enhanced electric attraction between the two phases. Consequently, sharply increasing Sr adsorption was found at higher pH.

3.2.2. Effect of Competitive Ions

The presence of cations coexisting with Sr^{2+} produces competition for available adsorption sites. Therefore, it is important to investigate the competitive influence of positive ions, especially divalent positive ions. Figure 3 shows the potential effects of competitive ions (Mg^{2+}, Ca^{2+}, Ba^{2+}) on Sr adsorption onto composite magnetic nanoparticles. The adsorption of Sr is dependent on the presence of cations and their concentrations in solution. The results demonstrated that with the increase of M/Sr (0–100), the removal of Sr^{2+} decreased, which indicated that Sr^{2+} adsorption is affected by the coexistence of other cations, especially when the M/Sr is greater than 100 (Sr removal < 20%). Furthermore, the Sr removal efficiency is dependent on the type of competing ions. For instance, at the same concentration, Mg hinders Sr uptake, whereas Ba has a lesser effect on Sr adsorption because of the size difference between the divalent ions.

The outer sphere complex was influenced more strongly by the ionic strength than the inner sphere complex [31]. The cations adsorbed by the outer-sphere association are sensitive to the ionic strength. By contrast, the cations that formed the inner-sphere complexes show an increase or no change in adsorption capacity with increasing ionic strength. In our system, Sr adsorption decreases with the increase of the ionic strength from 0.01 to 0.5 mol·L^{-1} at pH < 10, indicating that the outer-sphere mechanism was involved in the Sr adsorption at pH < 10 (Figure 2).

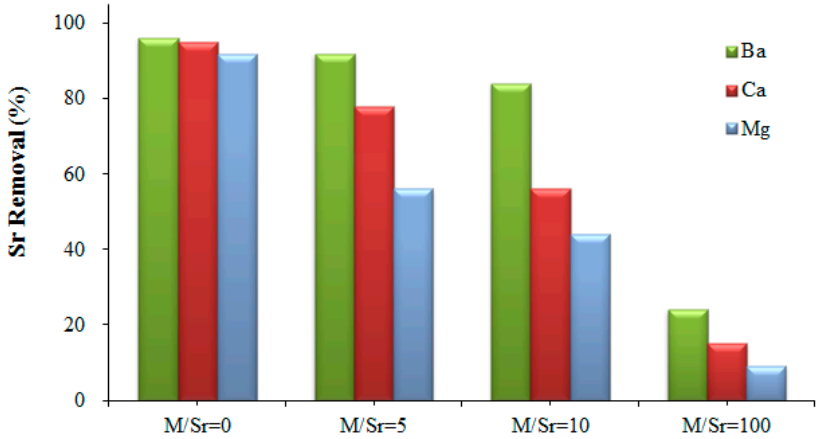

Figure 3. Effects of competitive ions on the Sr adsorption by the composite magnetic nanoparticles. Conditions: Adsorbent dose 5 g·L^{-1}, pH 10.25, *T* 298 K, ionic strength 0.5 mol·L^{-1}, contact time 120 min, Sr concentration 10 mg·L^{-1}.

3.3. Adsorption Kinetics

In large-scale or industrial plants, the rapid adsorption of the target element on the adsorbent is very important. Hence, the effect of contact time on the adsorption of Sr was examined to determine the time required for adsorption equilibrium. Figure 4a reveals the Sr adsorption with time at pH 10.25 and room temperature (ionic strength 0.5 mol·L^{-1}). The uptake of Sr was rapid in the first 60 min. After 120 min, the Sr adsorption did not change. Therefore, a contact time of 120 min was sufficient to reach equilibrium. Unless stated otherwise, the contact time was 120 min in the following experiments.

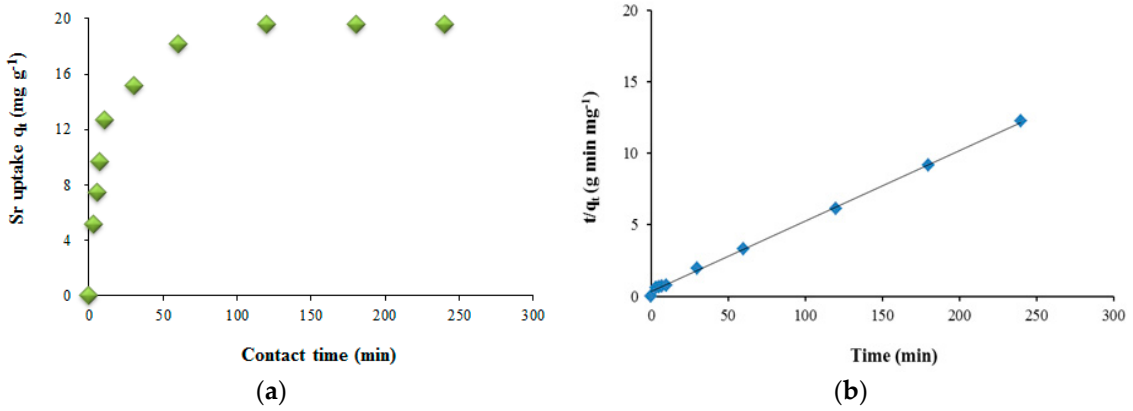

Figure 4. (**a**) Effect of the contact time on Sr adsorption; and (**b**) pseudo-second-order plot. Conditions: Adsorbent dose 5 g·L^{-1}, pH 10.25, *T* 298 K, ionic strength 0.5 mol·L^{-1}.

Two well-known kinetic models, pseudo-first-order [32] and pseudo-second-order [33], were used to fit the data shown in Figure 4a. Equations (5) and (6) present the linear forms of the pseudo-first-order and the pseudo-second-order kinetics, respectively:

$$\ln (q_e - q_t) = \ln q_e - k_1 t \quad (5)$$

$$\frac{t}{q_t} = \frac{1}{k_2 q_e^2} + \frac{t}{q_e} \quad (6)$$

where t is the contact time (min), q_e (mg·g^{-1}) and q_t (mg·g^{-1}) are the amounts of Sr^{2+} adsorbed at equilibrium and at time t, and k_1 (min^{-1}) and k_2 (g mg^{-1}·min^{-1}) are the rate constants of the pseudo-first-order and the pseudo-second-order kinetics, respectively. Figure 4b shows the plot of t/q_t versus t.

There is good linearity in the plot, with R^2 = 0.9989. This result indicates that the pseudo-second-order kinetic model yields a good fitting and suggests that the kinetics of Sr^{2+} adsorption on composite magnetic nanoparticles can be described by the pseudo-second-order equation.

3.4. Isotherm Modeling

Isotherm modeling is important for establishing an adsorption system and provides information on the capacity of the adsorbent or the amount required for removing a unit mass of pollutant under the designated conditions. The Freundlich [34] and Langmuir isotherms [35] are the most commonly used adsorption isotherms for describing the non-linear equilibrium of the adsorbate between the solution and adsorbent at a fixed temperature. Figure 5 presents the adsorption isotherms of Sr on the composite magnetic nanoparticles at different temperatures (298–318 K). The batch experiment data were fitted to the Langmuir and Freundlich isotherm models using the least squares method. The Langmuir isotherm model is obtained from a combination of the adsorption and the desorption rate equations, which can be written as follows [36]:

$$\frac{d\theta_t}{dt} = k_{ads} C_t N (1 - \theta_t) - k_d N \theta_t \quad (7)$$

where N is the maximum number of adsorption sites occupied by Sr and θ_t is the dimensionless surface coverage ratio. When the adsorption process reaches equilibrium, Equation (7) yields:

$$q_e = \frac{K_L q_m C_e}{1 + K_L C_e}, \quad (8)$$

where q_m is the maximum adsorption capacity (mg·g^{-1}), q_e is the amount of Sr adsorbed at equilibrium (mg·g^{-1}), and K_L is the Langmuir constant. Equation (9) shows the rearranged form yielded from Equation (8):

$$\frac{C_e}{q_e} = \frac{1}{K_L q_m} + \frac{C_e}{q_m} \quad (9)$$

The Freundlich isotherm model describes the relationship between the amount of Sr adsorbed by the composite magnetic nanoparticles (q_e, mg·g^{-1}) and the equilibrium concentration of Sr (C_e, mg·L^{-1}) in solution:

$$q_e = K_F C_e^{1/n} \quad (10)$$

where K_F and n are the Freundlich constants related to the adsorption capacity and the adsorption intensity, respectively.

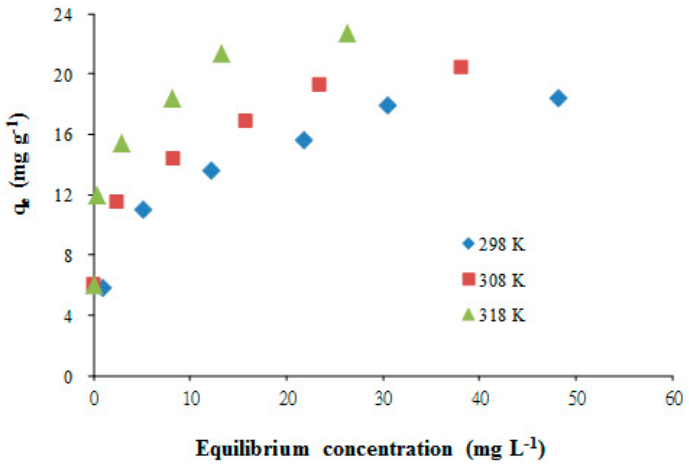

Figure 5. Sr adsorption isotherms on composite magnetic nanoparticles at 298, 308 and 318 K. Conditions: Adsorbent dose 5 g·L^{-1}, pH 10.25.

Figure 6a,b reveal linear plots of $\ln q_e$ versus $\ln C_e$ and C_e/q_e versus C_e. For each isotherm in Figure 6a, linear regression analysis was used for the isotherm data (K_F and n) treatment. A similar method was used for the values of q_m and K_L in Figure 6b.

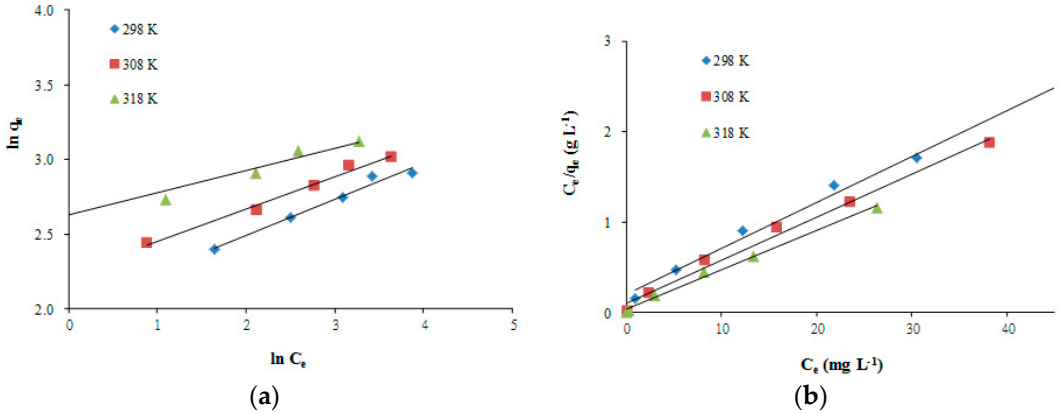

Figure 6. Linearized parameters of the adsorption isotherm models for Sr on the composite magnetic nanoparticles. (**a**) Freundlich isotherm model; (**b**) Langmuir isotherm model.

Table 1 shows the parameters of the Freundlich and Langmuir isotherm models for Sr adsorption on the composite magnetic nanoparticles at three temperatures (298, 308, and 318 K). The Langmuir model yields a better fit than the Freundlich model at the investigated temperatures. Moreover, the Sr adsorption capacity increases with temperature, suggesting an endothermic nature of the adsorption. In addition, the thermodynamic parameters can be determined from the changes of the thermodynamic equilibrium constant K and temperature [37,38]. For adsorption reactions, K is expressed as follows:

$$K = \frac{a_s}{a_e} = \frac{v_s}{v_e}\frac{C_s}{C_e} \tag{11}$$

where a_e is the activity of Sr in solution at equilibrium, a_s is the activity of adsorbed Sr, C_s is the surface concentration of Sr (mmol·g^{-1}) in the adsorbent, C_e is the Sr concentration in solution at equilibrium (mmol·mL^{-1}), v_e is the activity coefficient of the Sr in solution, and v_s is the activity coefficient of the adsorbed Sr. As the Sr concentration in the solution decreases to zero, K can be obtained by plotting $\ln(C_s/C_e)$ versus C_s and extrapolating C_s to zero [37]. The obtained straight line is fit to the data points by the least squares analysis. The intercept at the vertical axis yields the values of K. The changes of the adsorption standard free energy (ΔG°) can be calculated from the following equation:

$$\Delta G^o = -RT\ln K \tag{12}$$

where R is the universal gas constant (8.314 J·mol^{-1}·K^{-1}) and T is the absolute temperature (K). The average changes of the standard enthalpy (ΔH°) and entropy (ΔS°) of Sr adsorption onto the composite magnetic nanoparticles were determined by the following equation:

$$\ln K = \frac{\Delta S^o}{R} - \frac{\Delta H^o}{RT} \tag{13}$$

where ΔH° and ΔS° were calculated from the slope and the intercept, respectively, in the plot of $\ln K$ against $1/T$ [39]. These data are shown in Figure 7, and the thermodynamic parameters for the Sr adsorption process on the composite magnetic nanoparticles are provided in Table 2.

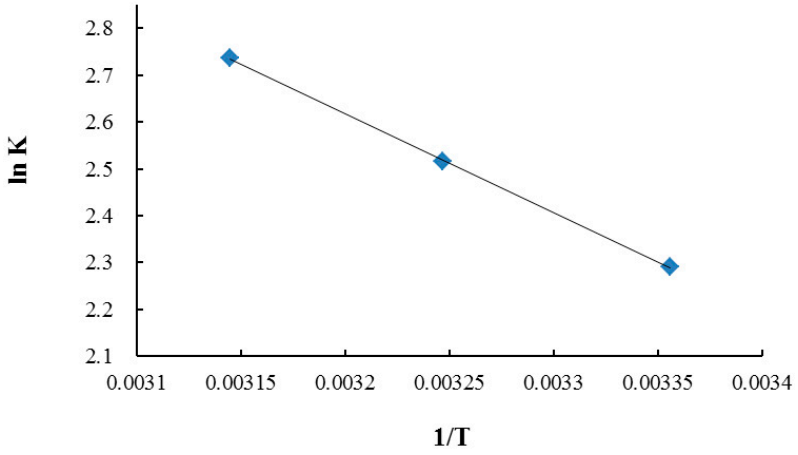

Figure 7. Plot of ln$K$ vs. $1/T$ for the estimation of the thermodynamic parameters for the adsorption of Sr on the composite magnetic nanoparticles.

Table 1. Parameters of the Freundlich and Langmuir adsorption isotherm models for Strontium (Sr) on the composite magnetic nanoparticles.

Temperature (K)	Freundlich			Langmuir		
	K_F	n	R^2	q_m	K_L	R^2
298	7.381	4.090	0.9788	19.72	0.248	0.9939
308	9.373	4.632	0.9853	21.05	0.439	0.9899
318	13.831	6.716	0.9744	23.04	1.130	0.9938

Table 2. Thermodynamic parameters for the adsorption of Sr on the composite magnetic nanoparticles.

Temperature (K)	Thermodynamic Constant			
	K (m·M^{-1})	ΔG° (kJ·mol^{-1})	ΔS° (J·mol^{-1}·K^{-1})	ΔH° (kJ·mol^{-1})
298	9.88	−5.68		
308	12.39	−6.45	9.38	2.11
318	15.43	−7.23		

The negative change in the adsorption standard free energy (ΔG° = −5.68, −6.45, and −7.23 kJ·mol^{-1} at 298, 308, and 318 K, respectively) shows that the adsorption reaction is a spontaneous process [37]. The absolute value of ΔG° increased with the increase of temperature, indicating that the adsorption is more spontaneous at higher temperature. The positive ΔH° values (2.11 kJ·mol^{-1}) confirm the endothermic nature of the adsorption process, which is also evidenced by the enhanced Sr adsorption at higher temperature. In addition, the positive value of ΔS° (9.38 J·mol^{-1}·K^{-1}) indicates that the randomness was increased at the solid-solution interface during Sr adsorption [40].

3.5. Comparison of the Sr Adsorption Capacity with Other Adsorbents

The adsorption capacity of the composite magnetic nanoparticles for the removal of Sr was compared with various adsorbents (Table 3). Our composite magnetic nanoparticles efficiently uptake Sr in aqueous solution. The maximum adsorption of Sr at 318 K on the composite magnetic nanoparticles was 23.04 mg Sr/g $CuFe_2O_4$ (calculated based on the Langmuir isotherm). This adsorption capacity is higher than several of the listed adsorbents, including ammonium molybdophosphate polyacrylonitrile (16.6 mg·g^{-1}) [13], montmorillonite (13.3 mg·g^{-1}) [8], phosphate-modified montmorillonite (12.6 mg·g^{-1}) [8], magnetic Fe3O4 particle-modified sawdust (12.6 mg·g^{-1}) [41], and hydrous ferric oxide (6.9 mg·g^{-1}) [21].

Table 3. Comparison of the Sr adsorption capacity among different adsorbents at various temperatures.

Adsorbents	pH	Temperature (K)	Sr adsorption Capacity ($mg \cdot g^{-1}$)	References
FeOOH (BT1)	10.50	318	39.8	[29]
FeOOH (BT1)	10.50	303	38.5	[29]
FeOOH (BT1)	10.50	293	32.9	[29]
FeOOH (BT9)	11.22	323	29.9	[30]
FeOOH (BT9)	11.22	303	28.0	[30]
FeOOH (BT9)	11.22	288	27.0	[30]
Composite magnetic nanoparticles	10.25	318	23.0	This study
Composite magnetic nanoparticles	10.25	308	21.1	This study
Composite magnetic nanoparticles	10.25	298	19.7	This study
Ammonium molybdophosphate polyacrylonitrile	5.01	293	16.6	[13]
Phosphate-modified montmorillonite	-	298	12.6	[8]
Magnetic Fe_3O_4 particles modified sawdust	6.74	293	12.6	[41]
Hydrous ferric oxide	10.01	293	6.9	[21]
Dolomite	5.50	293	1.2	[22]

3.6. Sr Removal from Seawater

To evaluate the adsorption performance of Sr from real seawater by the composite magnetic nanoparticles, a sample of seawater collected in Kaohsiung, Taiwan was reacted with the adsorbents. Four pH conditions (pH 10.37, 8.21, 6.09, and 3.13) were used to test the adsorption performance of Sr from the seawater (initial pH 8.21) by the composite magnetic nanoparticles. The Sr removal reached 62.3% in actual seawater media (pH 8.21) (Table 4). The Sr removal decreased markedly, to 17.5% and 2.4%, after the pH was adjusted to 6.09 and 3.13, respectively. The Sr removal reached 86.5% when the pH was adjusted to more alkaline conditions (pH 10.37), which proved that Sr could be easily absorbed in neutral to alkaline conditions due to the electric attraction.

Table 4. Sr removal in seawater using the composite magnetic nanoparticles.

Matrix	Adsorption pH	Sr ($mg \cdot L^{-1}$)		
		before Adsorption ($mg \cdot L^{-1}$)	after Adsorption ($mg \cdot L^{-1}$)	Removal (%)
Seawater	10.37 (adjusted pH)	7.98	1.08	86.5
	8.21 (natural pH)	7.98	3.01	62.3
	6.09 (adjusted pH)	7.98	6.58	17.5
	3.13 (adjusted pH)	7.98	7.79	2.4

Notes: Amount of adsorbent = 0.05 g, Volume = 10 mL, Temperature = 298 K, Time = 30 min. Detection limit for Sr: 0.017 $mg \cdot L^{-1}$.

4. Conclusions

The composite magnetic nanoparticles ($CuFe_2O_4$) were successfully applied to remove Sr^{2+} from aqueous solutions. The pH effect, influence of competitive ions, ionic strength, kinetics, isotherms, equilibrium, and thermodynamics of Sr adsorption were examined. The structural characterization indicates that the crystalline pattern of the composite magnetic nanoparticles was $CuFe_2O_4$. The SEM images and zeta meter show that the particle size of the composite magnetic nanoparticles range between 20 and 120 nm. The second-order model accurately fits the Sr adsorption kinetics for the adsorbent, and the data agree with the Langmuir adsorption isotherm model. Additionally, thermodynamic studies demonstrate that the adsorption process was endothermic and spontaneous in nature. The optimal adsorption efficiency was greater than 86.5% at pH 10.37, indicating that the synthesized composite magnetic nanoparticles have the potential for fast and effective Sr removal from seawater.

Acknowledgments: This research is sponsored by Shanghai Normal University under the Grant No. SK201614 and SK201615. The work is also supported by the Shanghai Gaofeng and Gaoyuan Project for University Academic Program Development. The authors would like to thank Wei-The Jiang, Po-Shu Lee and Yi-Liang Wang for their assistance with the XRD and SEM analysis under project MOST103-2119-M006-004.

Author Contributions: All authors contributed equally to this work. Yao-Jen Tu and Chen-Feng You conceived and designed the experiments. Yao-Jen Tu, Zhonghao Zhang, Yanping Duan, Jing Fu and Di Xu analyzed the data; Yao-Jen Tu and Zhonghao Zhang wrote the paper.

Conflicts of Interest: The authors declare no conflict of interest.

References

1. Baisden, P.A.; Choppin, G.R. Nuclear waste management and the nuclear fuel cycle. In *Radiochemistry and Nuclear Chemistry*; Encyclopedia of Life Support Systems (EOLSS): Oxford, UK, 2007.
2. U.S. Environmental Protection Agency (USEPA). *EPA Facts about Strontium-90*; USEPA: Washington, DC, USA, 2002.
3. Gerke, T.L.; Little, B.J.; Luxton, T.P.; Scheckel, K.G.; Maynard, J.B. Strontium concentrations in corrosion products from residential drinking water distribution systems. *Environ. Sci. Technol.* **2013**, *47*, 5171–5177. [CrossRef] [PubMed]
4. Chegrouche, S.; Mellah, A.; Barkat, M. Removal of strontium from aqueous solutions by adsorption onto activated carbon: Kinetic and thermodynamic studies. *Desalination* **2009**, *235*, 306–318. [CrossRef]
5. Dahl, S.G.; Allain, P.; Marie, P.J.; Mauras, Y.; Boivin, G.; Ammann, P.; Tsouderos, Y.; Delmas, P.D.; Christiansen, C. Incorporation and distribution of strontium in bone. *Bone* **2001**, *28*, 446–453. [CrossRef]
6. Nielsen, S.P. The biological role of strontium. *Bone* **2004**, *35*, 583–588. [CrossRef] [PubMed]
7. Mangano, J.J.; Sherman, J.D. Elevated in vivo strontium-90 from nuclear weapons test fallout among cancer decedents: A case-control study of deciduous teeth. *Int. J. Health Serv.* **2011**, *41*, 137–158. [CrossRef] [PubMed]
8. Ma, B.; Oh, S.; Shin, W.S.; Choi, S.J. Removal of Co^{2+}, Sr^{2+} and Cs^{+} from aqueous solution by phosphate-modified montmorillonite (PMM). *Desalination* **2011**, *276*, 336–346. [CrossRef]
9. Ambashta, R.D.; Sillanpää, M.E.T. Membrane purification in radioactive waste management: A short review. *J. Environ. Radioact.* **2012**, *105*, 76–84. [CrossRef] [PubMed]
10. U.S. Department of Health and Human Services. *Toxicological Profile for Strontium*; Public Health Service, Agency for Toxic Substances and Disease Registry: Washington, DC, USA, 2004.
11. Zhang, L.; Wei, J.Y.; Zhao, X.; Li, F.Z.; Jiang, F.; Zhang, M. Strontium(II) adsorption on Sb(III)/Sb_2O_5. *Chem. Eng. J.* **2015**, *267*, 245–252. [CrossRef]
12. Raut, D.R.; Mohapatra, P.K.; Manchanda, V.K. A highly efficient supported liquid membrane system for selective strontium separation leading to radioactive waste remediation. *J. Membr. Sci.* **2012**, *390–391*, 76–83. [CrossRef]
13. Park, Y.; Lee, Y.C.; Shin, W.S.; Choi, S.J. Removal of cobalt, strontium and cesium from radioactive laundry wastewater by ammonium molybdophosphate–polyacrylonitrile (AMP–PAN). *Chem. Eng. J.* **2010**, *162*, 685–695. [CrossRef]
14. Murthy, Z.V.P.; Parmar, S. Removal of strontium by electrocoagulation using stainless steel and aluminum electrodes. *Desalination* **2011**, *282*, 63–67. [CrossRef]
15. Faghihian, H.; Iravani, M.; Moayed, M.; Ghannadi-Maragheh, M. Preparation of a novel PAN–zeolite nanocomposite for removal of Cs^{+} and Sr^{2+} from aqueous solutions: Kinetic, equilibrium, and thermodynamic studies. *Chem. Eng. J.* **2013**, *222*, 41–48. [CrossRef]
16. Cho, Y.C.; Komarneni, S. Cation exchange equilibria of cesium and strontium with K-depleted biotite and muscovite. *Appl. Clay Sci.* **2009**, *44*, 15–20. [CrossRef]
17. Sen Gupta, S.; Bhattacharyya, K.G. Adsorption of heavy metals on kaolinite and montmorillonite: A review. *Phys. Chem. Chem. Phys.* **2012**, *14*, 6698–6723. [CrossRef] [PubMed]
18. Tu, Y.J.; You, C.F.; Chang, C.K.; Chan, T.S.; Li, S.H. XANES evidence of molybdenum adsorption onto novel fabricated nano-magnetic $CuFe_2O_4$. *Chem. Eng. J.* **2014**, *244*, 343–349. [CrossRef]
19. Cao, C.Y.; Qu, J.; Yan, W.S.; Zhu, J.F.; Wu, Z.Y.; Song, W.G. Low-cost synthesis of flowerlike α-Fe_2O_3 nanostructures for heavy metal ion removal: Adsorption property and mechanism. *Langmuir* **2012**, *28*, 4573–4579. [CrossRef] [PubMed]
20. Tu, Y.J.; You, C.F.; Chang, C.K. Conversion of waste Mn-Zn dry battery as efficient nano-adsorbents for hazardous metals removal. *J. Hazard. Mater.* **2013**, *258–259*, 102–108. [CrossRef] [PubMed]

21. Small, T.D.; Warren, L.A.; Ferris, F.G. Influence of ionic strength on strontium sorption to bacteria, Fe(III) oxide, and composite bacteria Fe(III) oxide surfaces. *Appl. Geochem.* **2001**, *16*, 939–946. [CrossRef]
22. Ghaemi, A.; Torab-Mostaedi, M.; Ghannadi-Maragheh, M. Characterizations of strontium(II) and barium(II) adsorption from aqueous solutions using dolomite powder. *J. Hazard. Mater.* **2011**, *190*, 916–921. [CrossRef] [PubMed]
23. Krupicka, S.; Novak, P. Oxide spinels. *Handb. Ferromagn. Mater.* **1982**, *3*, 189–304.
24. Tu, Y.J.; You, C.F.; Chang, C.K.; Wang, S.L.; Chan, T.S. Adsorption behavior of As(III) onto a copper ferrite generated from printed circuit board industry. *Chem. Eng. J.* **2013**, *225*, 433–439. [CrossRef]
25. Tu, Y.J.; You, C.F.; Chang, C.K. Kinetics and thermodynamics of adsorption for Cd on green manufactured nano-particles. *J. Hazard. Mater.* **2012**, *235–236*, 116–122. [CrossRef] [PubMed]
26. Tu, Y.J.; Chang, C.K.; You, C.F.; Lou, J.C. Recycling of Cu powder from industrial sludge by combined acid leaching, chemical exchange and ferrite process. *J. Hazard. Mater.* **2010**, *181*, 981–985. [CrossRef] [PubMed]
27. Tu, Y.J.; You, C.F.; Chang, C.K.; Wang, S.L.; Chan, T.S. Arsenate adsorption from water using a novel fabricated copper ferrite. *Chem. Eng. J.* **2012**, *198–199*, 440–448. [CrossRef]
28. Denizli, A.; Salih, B.; Piskin, E. New sorbents for removal of heavy metal ions: Diamine-glow-discharge treated polyhydroxyethylmethacrylate microspheres. *J. Chromatogr. A* **1997**, *773*, 169–178. [CrossRef]
29. Liu, C.H.; Shih, Y.J.; Huang, Y.H.; Huang, C.P. Kinetic and thermodynamic studies for adsorptive removal of Sr^{2+} using waste iron oxide. *J. Taiwan Inst. Chem. Eng.* **2014**, *45*, 914–920. [CrossRef]
30. Tu, Y.J.; You, C.F.; Chen, Y.R.; Huang, C.P.; Huang, Y.H. Application of recycled iron oxide for adsorptive removal of strontium. *J. Taiwan Inst. Chem. Eng.* **2015**, *53*, 92–97. [CrossRef]
31. Namasivayam, C.; Prathap, K. Uptake of molybdate by adsorption onto industrial solid waste Fe(III)/Cr(III) hydroxide: Kinetic and equilibrium studies. *Environ. Technol.* **2006**, *27*, 923–932. [CrossRef] [PubMed]
32. Lagergren, S. *Zur Theorie der Sogenannten Adsorption geloester Stoffe*; PA Norstedt & Söner: Stockholm, Sweden, 1898; Volume 24, pp. 1–39.
33. Ho, Y.S.; McKay, G. The kinetics of sorption of divalent metals ions onto sphagnum moss peat. *Water Res.* **2000**, *34*, 735–742. [CrossRef]
34. Freundlich, H.M.F. Ueber die adsorption in loesungen (Adsorption in solution). *J. Phys. Chem.* **1906**, *57*, 384–470.
35. Langmuir, I. The adsorption of gases on plane surfaces of glass, Mica and Platinum. *J. Am. Chem. Soc.* **1918**, *40*, 1361–1368. [CrossRef]
36. Chiron, N.; Guilet, R.; Deydier, E. Adsorption of Cu(II) and Pb(II) onto a grafted silica: Isotherms and kinetic models. *Water Res.* **2003**, *37*, 3079–3086. [CrossRef]
37. Li, Y.H.; Di, Z.; Ding, J.; Wu, D.; Luan, Z.; Zhu, Y. Adsorption thermodynamic, kinetic and desorption studies of Pb^{2+} on carbon nanotubes. *Water Res.* **2005**, *39*, 605–609. [CrossRef] [PubMed]
38. Khan, A.A.; Singh, R.P. Adsorption thermodynamics of carbofuran on Sn (IV) arsenosilicate in H^+, Na^+ and Ca^{2+} forms. *Colloids Surf.* **1987**, *24*, 33–42. [CrossRef]
39. Aksu, Z. Determination of the equilibrium, kinetic and thermodynamic parameters of the batch biosorption of nickel(II) ions onto chlorella vulgaris. *Process Biochem.* **2002**, *38*, 89–99. [CrossRef]
40. Yan, L.G.; Xu, Y.Y.; Yu, H.Q.; Xin, X.D.; Wei, Q.; Du, B. Adsorption of phosphate from aqueous solution by hydroxy-aluminum, hydroxy-iron and hydroxy-iron–aluminum pillared bentonites. *J. Hazard. Mater.* **2010**, *179*, 244–250. [CrossRef] [PubMed]
41. Cheng, Z.; Gao, Z.; Ma, W.; Sun, Q.; Wang, B.; Wang, X. Preparation of magnetic Fe_3O_4 particles modified sawdust as the adsorbent to remove strontium ions. *Chem. Eng. J.* **2012**, *209*, 451–457. [CrossRef]